Available online at www.sciencedirect.com
ScienceDirect
Journal of Nuclear Materials 357 (2006) 198–205
journal of nuclear materials
www.elsevier.com/locate/jnucmat

A NRA study of temperature and heavy ion irradiation effects on helium migration in sintered uranium dioxide

G. Martin [a], P. Garcia [b,*], H. Labrim [a], T. Sauvage [a], G. Carlot [b], P. Desgardin [a], M.F. Barthe [a], J.P. Piron [b]

[a] Centre d'Etudes et de Recherches par Irradiation, 3A rue de la Férollerie, 45071 Orléans cedex 2, France
[b] CEA, CE de Cadarache, DEN/DEC/SESC/LLCC, Bât. 151, 13108 Saint-Paul-lez-Durance cedex, France

Received 21 December 2005; accepted 23 June 2006

Abstract

Helium implanted uranium dioxide sintered samples were studied using nuclear reaction analysis prior to and following heavy ion irradiations and temperature anneals at 800 °C and 1100 °C. The results show that the heavy ion irradiations do not produce measurable long range movement of helium atoms. However, the ion irradiations do affect the behaviour of helium during subsequent temperature anneals. As regards the 800 °C anneal, the reduced mobility of helium in the ion-irradiated samples is interpreted as resulting from enhanced helium atom segregation produced by the ion-irradiation. Conversely at 1100 °C, the initial heavy ion irradiation appears to produce a greater than expected movement of helium within the bulk of the sample which could be an indication of defect assisted helium diffusion. Thermal diffusion coefficients are also reported at 800 °C and 1100 °C based on an analysis using a one-dimensional diffusion model.

PACS: 61.82.Ms; 66.30.Jt; 66.30.Xj

1. Introduction

The behaviour of fission gases Xe and Kr produced in nuclear oxide fuels has been extensively studied due to their potential effects on the structural and mechanical properties of fuel elements (see for instance [1] or [2]). Helium is another rare gas produced in-pile. Moreover, a substantial quantity is expected to form under long term storage conditions as a result of the alpha decay of certain actinides. To help predict the evolution of irradiated oxide fuel, the behaviour of helium implanted in sintered uranium dioxide (UO_2) disks was looked at in previous studies [3–5]. A NRA (nuclear reaction analysis) technique using the $^3He(d,\alpha)^1H$ reaction enabled the study of ^3He depth profile changes in UO_2 sintered samples at various annealing stages. Results showed that helium is mobile in implanted polycrystalline samples at temperatures as low as 600 °C. He bubble precipitation was then found to

* Corresponding author. Tel.: +33 4 42 25 41 88; fax: +33 4 42 25 13 37.
E-mail address: garciap@drncad.cea.fr (P. Garcia).

0022-3115/$ - see front matter © 2006 Elsevier B.V. All rights reserved.
doi:10.1016/j.jnucmat.2006.06.021

predominate up to 1000 °C. At 1100 °C however, He release resumed unhindered [5]. Large helium release fractions were also observed in neutron irradiated oxide fuels at or around this threshold temperature and above [6].

However, fission fragments produced in-pile or alpha particles produced as a result of the decay of actinides during the storage of used fuels are likely to impact the behaviour of helium. These effects are studied in the work presented here. In particular, we wish to ascertain whether electronic energy loss mechanisms alone are capable of inducing athermal, long range movement of He atoms. To this end, ^{3}He was implanted at two different depths, 0.3 μm and 2 μm. Samples were irradiated with high energy heavy ions in order to produce defects essentially through electronic energy loss mechanisms at depths of a few micrometers from the samples' surface. The ^{3}He(d,α)^{1}H nuclear reaction analysis method was used to determine helium depth profiles before and after annealing at 800 °C and 1100 °C. The He depth profile changes measured as a function of the annealing temperature and heavy ion irradiation conditions are compared and discussed.

2. Experimental

2.1. Sample preparation and helium implantations

Four sintered uranium dioxide disks were polished on one side. The thickness of the disks was approximately 300 μm and their diameter 8.2 mm. After polishing, the disks were annealed at 1700 °C in a H_2 atmosphere (1.7 vol.% H_2O) for 24 h to remove the damage caused by polishing and insure that the samples were of stoichiometric composition. The average grain size following the 1700 °C anneal was estimated at approximately 24 μm. Two of the four UO_2 disks (G1, G2) were implanted simultaneously at room temperature with 0.1 MeV $^3He^+$ ions to a fluence of 0.56×10^{16} at. cm^{-2} using the 400 kV implanter at CSNSM Orsay. Both other disks (G3, G4) were implanted to a fluence of 1.7×10^{16} at. cm^{-2} with 1 MeV $^3He^+$ ions using the 3.5 MV Van de Graaff accelerator at CERI Orléans. Fluences were chosen to obtain similar helium concentrations (0.3 at.%) at the depth profile peak. Details concerning polycrystalline sample E4 allude to in Section 3.4 can be found in Ref. [5].

2.2. Heavy ion irradiations

Only two samples were irradiated at room temperature with heavy ions, G2 and G4. G2 was irradiated to a fluence of 0.13×10^{16} at. cm^{-2} with 220 MeV $^{79}Br^{12+}$ ions and G4 was irradiated to a fluence of 0.14×10^{16} at. cm^{-2} with 250 MeV $^{127}I^{14+}$ ions. Both ion irradiations were performed at the IRES Vivitron accelerator in Strasbourg. Of course, these energies are greater than fission fragment energies, typically around 120 MeV (respectively 70 MeV) for the lighter (respectively heavier) of the two fission fragments. However, the energy loss corresponding to the bromine irradiation in particular is very similar to that of fission fragments (typically 20 keV/nm) as can be seen from Table 1. The electronic energy loss associated with the iodine irradiation is somewhat greater than that of typical fission fragments, but these irradiation conditions were chosen so as to exacerbate effects associated with electronic excitation.

2.3. Annealing conditions

All the samples were annealed twice under reducing atmospheres (Ar, 10 vol.% H_2) at 800 °C

Table 1
Average electronic and nuclear energy losses in MeV μm^{-1} relative to initial helium implantations and heavy ion irradiations

		Depth x		
		$x < 1$ μm	1 μm $< x <$ 2.2 μm	$x >$ 2.2 μm
Helium 0.1 MeV	dE/dx el.	0.2	–	
	dE/dx nucl.	0.007	–	
Bromine 220 MeV	dE/dx el.	22	21	9
	dE/dx nucl.	0.04	0.04	0.5
Helium 1 MeV	dE/dx el.	0.6	0.3	–
	dE/dx nucl.	0.001	0.005	–
Iodine 250 MeV	dE/dx el.	32	30	15
	dE/dx nucl.	0.11	0.13	0.52

for 70 min and at 1100 °C for 25 min. They were furthermore annealed simultaneously and therefore subjected to identical temperature cycles. NRA analyses were performed prior to and following each anneal to determine He depth profiles. The different analyses were performed on different areas of the samples.

2.4. Defects introduced in samples

The defect profiles produced by nuclear collisions during the helium implantations and heavy ion irradiations were calculated with SRIM 2003. The mean projected ranges of the bromine and iodine ions were found to be equal to respectively 13 μm and 11 μm. Results show that in the regions where helium was implanted (within 3 μm from the sample surface), the cumulated damage caused by nuclear collisions remains low: less than 1 dpa. Furthermore, the damage caused through nuclear collisions by the initial helium implantation or the heavy ion irradiation are roughly equivalent.

The electronic and nuclear stopping powers for the various implanted species are also reported (Table 1). The three regions at which the stopping powers were estimated correspond to areas near the surface where G1 and G2 were implanted, towards the concentration peaks of samples G3 and G4 (implanted at a depth of 2 μm) and beyond it towards the tail end of the helium distributions. Table 1 shows that the predominant cause of energy loss is due to electronic interaction of the heavy ions used to irradiate the samples.

Under these conditions, it is probable that in the region extending from the samples' surface to a few micrometers away from it, electronic interaction of the high energy heavy ions with the matrix will also contribute to defect production. RAMAN measurements were done on a Jobin-YvonT64000 spectrometer in triple substractive configuration, under microscope (50× magnification), with the 647.1 nm krypton excitation line of 7 mW on the sample at CRMHT in Orléans. Samples G1 and G2 following the second annealing stage at 1100 °C were characterised. Results showed that the UO_2 peak at 445 cm^{-1} [7] was lower in the case of the ion-irradiated sample. This indicates that the disorder in the matrix is higher in the first micrometers from the sample surface after the ion-irradiation, and certainly well beyond the depth at which He was initially implanted. It further indicates that large amounts of defects have been created in an area where the heavy ions lose their energy essentially through electronic excitation.

2.5. NRA and helium depth profiles

The $^3He(d,\alpha)^1H$ nuclear reaction analysis method was used to determine helium concentrations at distances from the sample surface of up to 3.5 μm. The measurements were performed at the 3.5 MV Van de Graaff accelerator at CERI Orléans with an experimental set-up based on the simultaneous detection of both reaction products, α-particles and protons. Depth profiles were characterised using a deuteron beam of 500×500 μm^2 at 750 keV. Other details pertaining to the method (experimental set-up, energy calibration of the detectors and depth profile determination) are described in [4,5].

3. Results and discussion

3.1. Samples prior to annealing

Results relative to all as-implanted samples prior to annealing are summarised in Table 2. These results (see also Fig. 1) show that the maximum He concentrations corresponding to the shallow and deeper implants are identical and that the helium depth profiles relating to the ion-irradiated disks are very similar to those relating to the un-irradiated samples. Tables 3 and 4 provide data equivalent to Table 2, for samples G1, G2, G3 and G4 following annealing at 800 °C and 1100 °C respectively.

For the shallower implants (G1 and G2), the NRA technique is capable of detecting He movement over distances at or above 40 nm. This result would appear to differ from those of Hocking et al. [8] relative to radiation induced diffusion (RID) of iodine. In this work, UO_2 samples initially implanted with 930 keV iodine ions to a dose of 10^{13} ions cm^{-2}, were further irradiated with 72 MeV ^{127}I ions to doses of 5×10^{14} ions cm^{-2} and 5×10^{15} ions cm^{-2}. Secondary ion mass spectrometry (SIMS) investigations revealed that the heavy ion irradiations induced substantial diffusive spreading of the initial iodine profile. An analogy was then drawn with athermal in-reactor diffusion of various other species including rare gases and the uranium atoms indigenous to the fuel matrix. From previous in-pile studies [9–11], chemical species were thought to diffuse athermally at rates proportional to the fission density. Hocking et al. developed this analogy and derived from their ion-

Table 2
Characteristics of He depth profiles prior to annealing

Sample characteristics	Sample name			
	G1 0.1 MeV He implantation	G2 0.1 MeV He implantation further irradiated with 220 MeV Br ions	G3 1 MeV He implantation	G4 1 MeV He implantation further irradiated with 250 MeV I ions
Maximum [He] (at.%)	0.28 ± 0.01	0.28 ± 0.01	0.29 ± 0.01	0.30 ± 0.01
Position of maximum (μm)	0.30 ± 0.03	0.30 ± 0.03	2.0 ± 0.1	1.9 ± 0.1
Projected range (μm)	0.32 ± 0.03	0.33 ± 0.03	1.8 ± 0.1	1.8 ± 0.1
FWHM (μm)	0.25 ± 0.03	0.28 ± 0.03	0.7 ± 0.1	0.7 ± 0.1
He content (10^{16} at. cm^{-2})	0.56 ± 0.03	0.56 ± 0.03	1.69 ± 0.06	1.70 ± 0.06

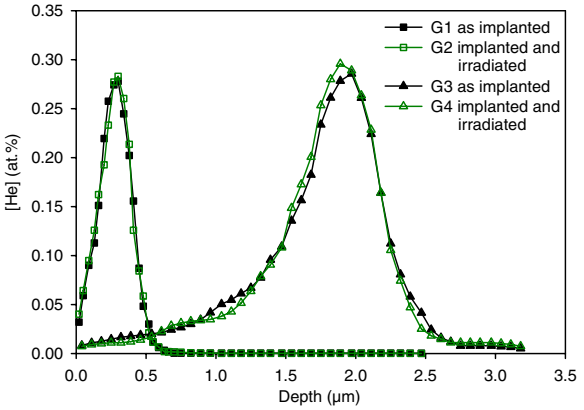

Fig. 1. ^{3}He depth profiles of samples implanted with helium at 0.1 MeV and 1 MeV; G1 and G3 are as-implanted whereas G2 and G4 were further ion irradiated with Br and I ions respectively.

irradiation experiment a proportionality constant A between the athermal diffusion coefficient and the fission density of between 0.5×10^{-29} cm^5 and 2×10^{-29} cm^5. This figure compares to 2×10^{-30} cm^5 found by Turnbull [9] for fission gases and iodine. Assuming the same analogy as Hocking et al. between fission rate in-pile and irradiation dose in an accelerator experiment and assuming A values quoted above, one would have expected a broadening of the He profile of anything between 20 nm and 60 nm. This is clearly not observed here.

It is however entirely possible that at these He concentrations, the heavy-ion irradiation induces both He movement and structural defects within the fuel matrix which together combine to produce He bubbles following a mechanism akin to heterogeneous nucleation [12]. In Hocking's work, iodine was studied at concentrations low enough so as not to induce segregation or trapping phenomena.

3.2. 800 °C anneal

It can be seen from Fig. 2 that almost all the helium contained in G1 (which was not irradiated with heavy ions) has been released due to extensive He migration. Data provided in Table 3 indicate a helium loss of approximately 90%. A much greater proportion of helium remains subsequent to annealing at 800 °C in sample G2, which had been irradiated with heavy ions.

Helium depth profiles for G3 and G4 obtained after annealing for 70 min at 800 °C also differ

Table 3
Characteristics of He depth profiles following annealing at 800 °C for 70 min

Sample characteristics	Sample name			
	G1 0.1 MeV He implantation	G2 0.1 MeV He implantation further irradiated with 220 MeV Br ions	G3 1 MeV He implantation	G4 1 MeV He implantation further irradiated with 250 MeV I ions
Maximum [He] (at.%)	0.03 ± 0.01	0.22 ± 0.01	0.20 ± 0.01	0.31 ± 0.01
Position of maximum (μm)	0.20 ± 0.03	0.30 ± 0.03	1.8 ± 0.1	1.9 ± 0.1
Projected range (μm)	0.27 ± 0.03	0.37 ± 0.03	1.6 ± 0.1	1.8 ± 0.1
FWHM (μm)	0.23 ± 0.03	0.18 ± 0.03	0.9 ± 0.1	0.5 ± 0.1
He content (10^{16} at. cm^{-2})	0.07 ± 0.03	0.31 ± 0.03	1.52 ± 0.03	1.67 ± 0.03
He desorption rate (%)	90 ± 4	45 ± 4	10 ± 2	0 ± 2

Table 4
Characteristics of He depth profiles following annealing at 1100 °C for 25 min

Sample characteristics	Sample name	
	G3 1 MeV He implantation	G4 1 MeV He implantation further irradiated with 250 MeV I ions
Maximum He concentration (at.%)	0.18 ± 0.005	0.13 ± 0.006
Position of maximum (μm)	1.9 ± 0.1	1.9 ± 0.1
Projected range (μm)	1.8 ± 0.1	1.8 ± 0.1
FWHM (μm)	0.5 ± 0.1	1.0 ± 0.1
He content (10^{16} at. cm^{-2})	1.11 ± 0.03	1.11 ± 0.03
He desorption rate (%)	34 ± 3	34 ± 3

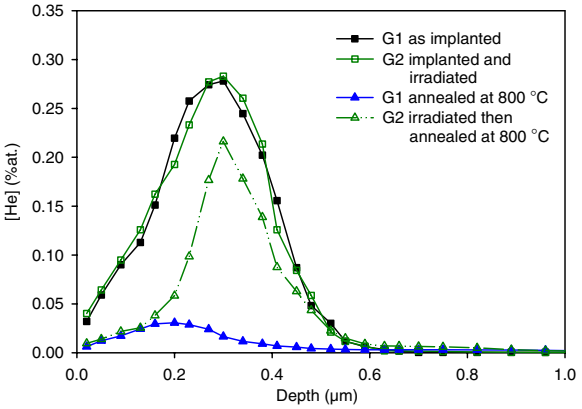

Fig. 2. ^{3}He depth profiles of samples implanted with 0.1 MeV helium ions, prior to and following an 800 °C anneal. Sample G2 was irradiated with Br ions prior to the anneal.

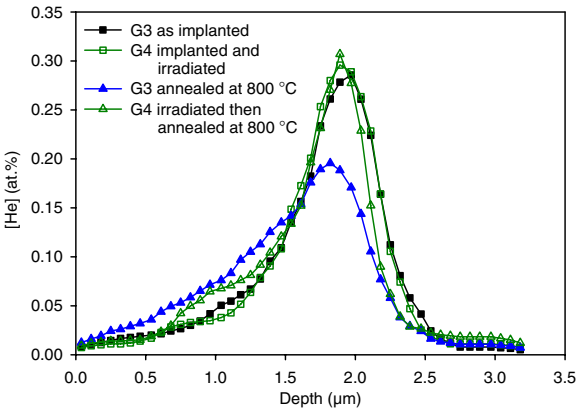

Fig. 3. ^{3}He depth profiles of samples implanted with 1 MeV helium ions, prior to and following an 800 °C anneal. Sample G4 was irradiated with I ions prior to the anneal.

substantially (Fig. 3). The helium depth profile for un-irradiated sample G3 appears to show diffusion type spreading between the profile maximum and the surface. By contrast, the helium profile for the ion irradiated G4 sample annealed at 800 °C is very similar to the profiles of as-implanted samples G3 and G4. The total helium content left in sample G4 deduced from the concentration profile is shown in Table 3 and indicates an almost insignificant loss of helium.

It is probable that at concentrations of 0.1–0.3 at.%, He bubble precipitation occurs. The differences observed in He behaviour between samples G3 and G4 (and G1 and G2) may be interpreted in terms of bubble precipitation. This phenomenon could be the direct consequence of the heavy ion irradiations as mentioned above, or it could be simply enhanced because of the presence of irradiation induced defects during subsequent thermal annealing. This is also seen from the FWHM values indicated in Table 3, which increases in the case of sample G3, indicating volume diffusion, but decreases in the case of the heavy ion-irradiated sample G4, possibly indicating greater susceptibility to bubble precipitation. Whether the defects created during the heavy ion irradiation are liable to trap individual helium atoms or whether trapping occurs because of enhanced bubble nucleation is clearly open to debate and could only be settled through extensive TEM work.

3.3. Samples annealed at 1100 °C

G1 and G2 were also annealed at 1100 °C for approximately 25 min, but in both cases almost all the He that they contained initially was released, thus precluding the generation of depth profiles. In this case, one can conclude that the heavy ion irradiation has no overall effect on He release and that thermal resolution of He trapped in bubbles or associated with irradiation induced defects becomes highly effective.

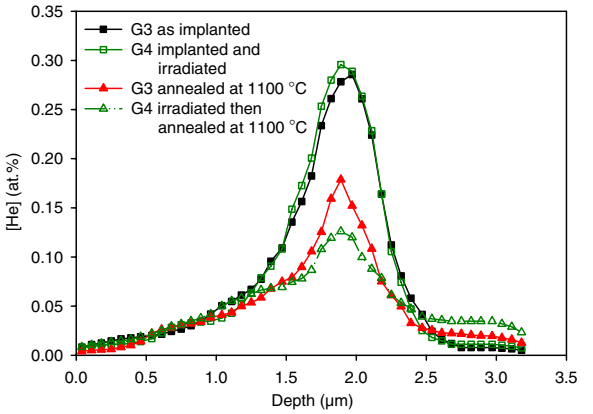

Fig. 4. ^{3}He depth profiles of samples implanted with 1 MeV helium ions, prior to 800 °C anneal and following an 1100 °C anneal. Sample G4 was irradiated with I ions prior to the 800 °C anneal.

Helium depth profiles of G3 and G4 following the second anneal (25 min at 1100 °C) are quite similar (Fig. 4) as are the overall He release fractions (approximately 35% for both samples). Over 1.5 μm from the surface of the sample, helium concentrations are similar to those found in the as-implanted samples. In both cases, diffusive spreading can be seen beyond the distribution peak and towards the bulk of the sample which is not due to low counting statistics.

At this temperature, it would appear that helium is more mobile as a result of the heavy ion irradiation, contrasting with observations at 800 °C. It was observed in previous experiments that at temperatures of 1100 °C, trapping which may have occurred at lower temperatures was off-set probably by thermal resolution [5]. This is entirely consistent with the results obtained here. However, there appears to be less He around the concentration profile maximum and more towards the surface and bulk of the specimen which has been ion irradiated. This can be interpreted as being due to enhanced diffusion caused by the presence of irradiation induced defects.

3.4. Model calculations

It was shown in a previous paper that the changes in concentration profiles seen here at 1100 °C, that reveal very little diffusive spreading, could be due to a direct release of helium through grain boundaries or other surface defects [5]. Grain boundary release is also a relevant mechanism in irradiated or alpha-doped materials [6]. He release via the grain boundaries was finally recently demonstrated by studying He behaviour using a microbeam [13]. Helium release via grain boundaries is probably also the main release mechanism in the present case for annealing experiments at 1100 °C at least.

To quantify this, the simple one-dimensional model used previously [5] was applied to calculating the concentration profile changes of samples which were not irradiated with Br or I ions. It cannot be overemphasised that the physical values deduced from such modelling do not reflect simple intrinsic material properties. The physical problem is an extremely complex one in which a great number of time dependent and non-linear phenomena are occurring simultaneously such as volume and grain boundary diffusion, bubble precipitation and growth, enhanced diffusion due to irradiation defects, etc. Simple modelling though serves the dual purpose of acting as a guide into understanding and de-correlating certain effects. It can also be used to generate data which are then compared to others obtained from experiments carried out under conditions which differ in terms of temperature, helium concentration or material microstructure.

The equation against which the data were fitted can be written as

$$\frac{\partial C(x,t)}{\partial t} = \frac{\partial}{\partial x}\left(D(x)\frac{\partial}{\partial x}C(x,t)\right) - k(x)C(x,t) - v\frac{\partial C}{\partial x} \quad (1)$$

in which the first term simulates space dependent volume diffusion. As described in [5], a direct loss term $k(x)$ is introduced in the diffusion equation. This term represents loss at three-dimensional defects at the surface of the samples such as fabrication pores intersecting the surface or grain boundaries at which accelerated diffusion is possible. As reported previously, k is assumed to be proportional to a first approximation to the volume diffusion coefficient and represents lateral diffusion. The variability of D and k with depth (see Fig. 5) is thought to result from the damage caused by the initial He implantation which could contribute to diffusion acceleration.

The third term which appears in Eq. (1) is interpreted as resulting from the fact that the initial He implantation is likely to induce a stress gradient in

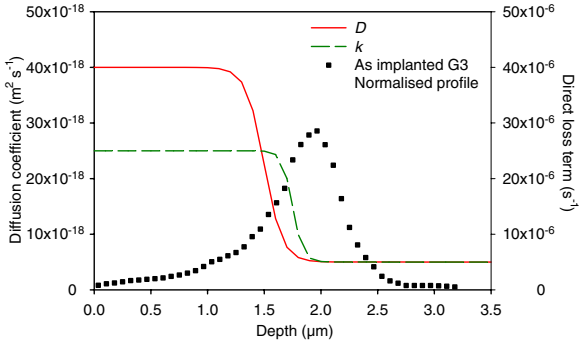

Fig. 5. Spatial variations of functions $D(x)$ (left-hand ordinate scale) and $k(x)$ (right-hand ordinate scale) used to fit the helium depth profile of G3 following annealing at 800 °C and normalised profile of as-implanted sample G3.

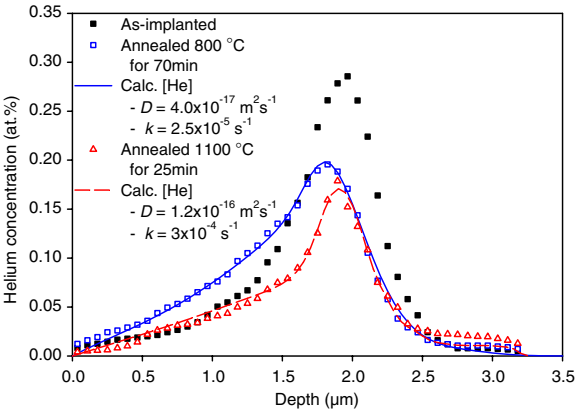

Fig. 6. Comparison between best-fit calculations and the helium depth profiles of G3 following annealing at 800 °C and 1100 °C.

the sample such that the stress field becomes compressive further away from the sample surface. The stress gradient gives rise to a driving force, the effect of which can be described through the use of a drift term in the diffusion equation [14].

As can be seen from Fig. 6, it was possible to fit the observed helium profile changes with v, D and k values reported in Fig. 5 and Table 5. At 1100 °C, no drift term was required to fit the experimental data, presumably because the heat treatment is likely to anneal out any stress gradient due to the initial He implantation.

Again, the numerical results should not be considered at their face value since some phenomena, notably bubble precipitation, are not described. The inferred diffusion coefficients therefore refer only to apparent diffusion coefficients.

D and k values at 1100 °C previously reported [5] have been reassessed and error bars determined. Values are also included in Table 5 despite the fact that they were obtained from helium implantations at the same energy but at lower doses (1.7×10^{16} ^{3}He cm^{-2} in the present study as opposed to 10^{16} ^{3}He cm^{-2} previously). The error bars reported in Table 5 where obtained by estimating, whenever possible, the intervals for each model parameter over which the calculated data yielded acceptable profiles, with regard to experimental errors both relating to the depth resolution and the He concentration. In some cases, the mechanism associated with a given model parameter is negligible in comparison to others which makes it only possible to determine an upper bound to the corresponding parameter.

Several comments can be made from Table 5. At 800 °C, the analysis of the data yields comparable diffusion coefficients in the higher and lower concentration experiments (samples G3 (this work) and E4

Table 5
D, k and v values obtained from the simulation of He depth profiles after different annealing stages of samples G3 and E4 (presented in a previous study [5]) implanted with 1 MeV ^{3}He ions

		Annealing temperature (°C)			
		800		1100	
		G3	E4 [5]	G3	E4 [5]
He dose (10^{16} ^{3}He cm^{-2})		1.7 ± 0.06	1.06 ± 0.02	1.7 ± 0.06	1.06 ± 0.02
Diffusion coefficient D (m^2 s^{-1})	[a]	$4 \pm 2 \times 10^{-17}$	$1.5 \pm 1 \times 10^{-17}$	$<1.5 \times 10^{-16}$	$5 \pm 3 \times 10^{-17}$
	[b]	$5 \pm 2 \times 10^{-18}$	$4 \pm 1 \times 10^{-18}$	$<2 \times 10^{-18}$	$<7 \times 10^{-18}$
Direct loss term k (s^{-1})	[a]	$2.5 \pm 1 \times 10^{-5}$	$6 \pm 2 \times 10^{-5}$	$4 \pm 1 \times 10^{-4}$	$4 \pm 1 \times 10^{-4}$
	[b]	$<2 \times 10^{-5}$	$<2 \times 10^{-5}$	$<3 \times 10^{-5}$	$<2 \times 10^{-5}$
Drift term v (m s^{-1})		$4 \pm 2 \times 10^{-11}$	$6 \pm 1 \times 10^{-11}$	$<3 \times 10^{-11}$	$<2 \times 10^{-11}$

[a] High diffusive region before maximum He concentration.
[b] Low diffusive region after maximum He concentration.

(see details in [5])). However in the low diffusive regions, the diffusion coefficient inferred from the analysis is approximately one order of magnitude lower than that towards the samples' surface.

Activation energies tentatively deduced from annealing experiments at 800 °C and 1100 °C are extremely low reflecting the fact that the diffusion coefficients inferred are enhanced due to the presence of defects introduced in the material as a result of the initial helium implantation. From the variation with depth of D and k, one would further assume that the defects enhancing the diffusion mechanism are produced as a result of incident He ions slowing down due to an electronic energy loss mechanism.

4. Conclusions

In this work, the combined effects of heavy ion irradiations and temperature on the behaviour of He in a UO_2 matrix are studied. He depth profiles in irradiated and non-irradiated He implanted samples are compared following various annealing sequences.

I or Br irradiations, simulating the effects of fission fragments, do not produce any detectable movement of helium in either of the samples. From this, we conclude that electronic excitation is alone not sufficient to produce substantial diffusive spreading of helium at concentrations similar to those expected in high duty fuel. This in itself is an important conclusion with regard to long term storage of spent fuels. The irradiations however do affect helium behaviour in subsequent annealing events.

For samples in which He was implanted closer to the surface, He release following annealing at 800 °C for 70 min is very substantially reduced as a result of an energetic ion irradiation. Release and movement appear to be completely inhibited in the case of samples in which He is located at greater depths.

At higher temperatures, i.e. 1100 °C, thermal resolution takes over and He thermal movement appears to resume. As regards the shallow implants most of the He contained in the samples is released. For samples in which He is implanted at greater depths, it would appear that the heavy ion irradiation enhances the mobility of He, presumably as a result of defect assisted diffusion.

In samples which were not irradiated with heavy ions, a one-dimensional diffusion model was used to infer diffusion coefficients at 800 °C and 1100 °C. It is shown that the initial He implantation produces effects which cause volume diffusion to appear to proceed at a higher rate in the region lying between the sample surface and the maximum He concentration.

Acknowledgements

The authors are grateful to the PRECCI programme, funded by CEA and EDF for supporting this work. This work is also the fruit of a collaborative programme under the auspices of the ACTINET network. Patrick Simon is thanked for his help and guidance in applying Raman spectroscopy to the UO_2 samples described in this paper and interpreting the results thereof.

References

[1] G.T. Lawrence, J. Nucl. Mater. 71 (1978) 195.
[2] Hj. Matzke, Radiat. Effects 53 (1980) 219.
[3] S. Guilbert, T. Sauvage, H. Erramli, M.F. Barthe, P. Desgardin, G. Blondiaux, C. Corbel, J.P. Piron, J. Nucl. Mater. 321 (2003) 121.
[4] T. Sauvage, H. Erramli, S. Guilbert, L. Vincent, M.F. Barthe, P. Desgardin, G. Blondiaux, C. Corbel, J.P. Piron, F. Labohm, J. Van Veen, J. Nucl. Mater. 327 (2004) 159.
[5] S. Guilbert, T. Sauvage, P. Garcia, G. Carlot, M.F. Barthe, P. Desgardin, G. Blondiaux, C. Corbel, J.P. Piron, J.M. Gras, J. Nucl. Mater. 327 (2004) 88.
[6] C. Ronchi, J.P. Hiernaut, J. Nucl. Mater. 325 (2004) 11.
[7] G. Allen, I. Butler, N. Tuan, J. Nucl. Mater. 144 (1987) 17.
[8] W.H. Hocking, R.A. Verrall, I.J. Muir, J. Nucl. Mater. 294 (2001) 45.
[9] J.A. Turnbull, C.A. Friskney, J.R. Findlay, F.A. Jonhson, A.J. Walter, J. Nucl. Mater. 107 (1982) 168.
[10] A. Höh, Hj. Matzke, J. Nucl. Mater. 48 (1973) 157.
[11] Hj. Matzke, Radiat. Effects 75 (1983) 317.
[12] R.M. Cornell, J.A. Turnbull, J. Nucl. Mater. 41 (1971) 87.
[13] T. Sauvage, P. Desgardin, G. Martin, P. Garcia, G. Carlot, H. Labrim, H. Khodja, P. Moretto, M.F. Barthe, G. Blondiaux, H. Erramli, J.P. Piron, Microstructure effects on He diffusion in sintered UO_2 by μNRA, Nucl. Instrum. and Meth. B 240 (2005) 271.
[14] J. Philibert, Atom movements, diffusion and mass transport in solids, Les éditions de physique, Les Ulis, 1991.